ChemComm

A Zn-S Aqueous Primary Battery with High Energy and Flat Discharge Plateau

SCHOLARONE™
Manuscripts

COMMUNICATION

A Zn-S Aqueous Primary Battery with High Energy and Flat Discharge Plateau †

Lian-Wei Luo,[a] Chong Zhang,[a,b,*] Xianyong Wu,[b] Changzhi Han,[a] Yunkai Xu,[b] Xiulei Ji,[b,*] Jia-Xing Jiang [a,*]

We demonstrate a disposable aqueous primary battery chemistry that comprises environmentally benign materials of the sulfur cathode and Zn anode in 1 M ZnCl$_2$ aqueous electrolyte. The Zn-S battery shows a high energy density of 1083.3 Wh kg^{-1} for sulphur with a flat discharge voltage plateau around 0.7 V. When operating at a high mass loading of 8.3 mg cm^{-2} for sulfur in the cathode, the battery exhibits a very high areal capacity of 11.4 mAh cm^{-2} and areal energy of 7.7 mWh cm^{-2}.

Aqueous zinc-metal batteries have attracted tremendous research interests due to the inherent safety of aqueous electrolytes as well as the advantages of Zn metal anode such as massive scale of manufacturing, high capacity, and good compatibility with aqueous electrolytes.[1-5] To date, several types of zinc-metal primary batteries have been commercialized such as Zn-MnO$_2$ dry batteries, Zn-Ag$_2$O$_2$ batteries, and Zn-air batteries.[6-8] Among these primary batteries, the alkaline Zn-MnO$_2$ battery has been widely used in the everyday life despite the ubiquitous utilization of rechargeable batteries. However, the relatively low theoretical capacity of MnO$_2$ cathode limits the energy density of alkaline Zn-MnO$_2$ batteries.[9-11] Hence, there is a need to explore new cathode materials for Zn metal primary batteries that offer higher energy density preferably at a lower cost.

Elemental sulfur (S) is mainly produced as a byproduct from the purification process of natural gas, petroleum and other minerals.[12-14] However, the current applications of sulfur such as the production of sulfuric acid, gunpowder, and rubber vulcanization cannot consume all the produced elemental sulfur. Therefore, the industry's involuntary manufacturing of sulfur and its insufficient consumption lead to a very low price, *i.e.*, 10% that of MnO$_2$ as well as the need to find new valuable applications of this material. The two-electron conversion reaction that generates sulfides renders S one of the most attractive electrodes in battery applications owing to its high theoretical specific capacity of 1671 mAh g^{-1}, albeit often with a moderate redox potential.[15-22] Several primary batteries based on elemental S cathode have been reported such as alkaline Al-S battery, Ca-S battery with an organic electrolyte,[23-26] demonstrating the great potential of sulfur cathode in primary batteries.

Herein, we demonstrate a Zn-S primary battery enabled by directly using sulfur as the cathode coupled with Zn metal anode in the mildly acidic 1 M ZnCl$_2$ electrolyte (pH=4.08). In this Zn-S battery, the elemental sulfur cathode can achieve its theoretical capacity with the discharge voltage around 0.7 V, corresponding to an energy density of 1083.3 Wh kg^{-1}. Impressively, this Zn-S primary battery could operate at a high mass loading of 8.3 mg cm^{-2} for S in the cathode, which realizes an areal capacity of 11.4 mAh cm^{-2}. This work reports a promising aqueous Zn-S primary battery with low cost and high energy density.

The sulfur cathode was prepared by infiltrating elemental sulfur into Ketjen Black (KB) to endow the cathode with high electronic conductivity. The energy dispersive X-ray spectroscopy (EDX) analysis revealed that the content of S in the KB-S composite is around 74.1% (Fig. 1a), which is very close to the result of 74.7% from the thermogravimetric analysis (Fig. S1). The elemental mapping demonstrated S was mixed well with the conductive KB. The X-ray diffraction pattern (XRD) also manifested the presence of element sulfur in the composite (Fig. S2). Both KB and the KB-S composite show nano-particle morphology with similar particle size (Fig. S3). The porosity of KB and KB-S composite was investigated by the N$_2$ sorption isotherms at 77.3 K. The calculated specific surface areas are 1346.9 and 19.3 m^2 g^{-1} for KB and KB-S composite, respectively (Fig. 1b). The sharply decreased surface area could be ascribed to the infiltration of S into the pores of KB, as evidenced by the decreased pore volume from 2.25 cm^3 g^{-1} for KB to 0.14 cm^3 g^{-1} for the KB-S composite (Fig. 1c).

a. Key Laboratory for Macromolecular Science of Shaanxi Province, Shaanxi Engineering Laboratory for Advanced Energy Technology, School of Materials Science and Engineering, Shaanxi Normal University, Xi'an, Shaanxi 710062, P. R. China.
E-mail: chongzhangabc@snnu.edu.cn; jiaxing@snnu.edu.cn
b. Department of Chemistry, Oregon State University, Corvallis, OR, 97331-4003, United States.
E-mail: david.ji@oregonstate.edu
†Electronic Supplementary Information (ESI) available: Details for synthesis and characterizations of the KB-S composition, TG curve, XRD patterns, SEM images, EDX spectrum, XPS spectra and EIS profiles. See DOI: 10.1039/x0xx00000x
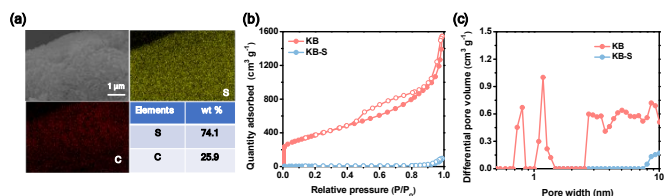
Fig.1 (a) The SEM image and the corresponding elemental mapping of KB-S composite. (b) Nitrogen adsorption-desorption isotherms collected at 77.3 K. (c) Pore size distribution.

The electrochemical performance of the Zn-S primary battery was firstly evaluated by galvanostatic discharge in different electrolytes in a two-electrode cell using the KB-S composite as cathode and Zn foil as anode. The Zn-S battery shows similar open circuit voltage around 1 V in different electrolytes (Fig. 2a). However, the discharge voltage and specific capacity of the sulfur cathode vary dramatically with the different aqueous electrolytes. The Zn-S battery shows the highest discharge voltage around 0.7 V in 1 M $ZnCl_2$ electrolyte with a high specific capacity of 1668 mAh g^{-1} based on the mass of S after subtracting the capacity contribution of KB (Fig. S4), corresponding to an energy density of 1083.3 Wh kg^{-1}, which is higher than that of the reported MnO_2 cathode (~370 Wh kg^{-1}) in alkaline Zn-MnO_2 primary battery.[27] We also assembled an aqueous Zn-S full cell by using limited Zn foil as the anode, and the mass ratio of Zn to sulfur is 2.2:1. This full cell achieved an energy density of 240 Wh kg^{-1} based on the mass of both the cathode and anode (Fig. S5). Please note that the plateau region accounts for 88.8% of the total energy density, indicating a consistent energy output during the practical application (Fig. S6). The different discharge voltages could be ascribed to the different interfacial charge transfer resistance (R_{ct}) of the KB-S composites in different

Fig. 2 (a) The discharge profiles of Zn-S batteries with different electrolytes at 50 mA g^{-1}. (b) EIS spectra of Zn-S batteries with different electrolytes. (c) Ex-situ XRD patterns of the pristine and discharged sulfur cathodes. (d) The HR-TEM image of the discharged sulfur cathode. (e) The elemental mapping of the discharged sulfur cathode. (f) Ex situ high-resolution XPS spectra of sulfur cathodes at different SOC, the discharge rate is 50 mA g^{-1}.

electrolytes, where the lowest R_{ct} was achieved in 1 M $ZnCl_2$ electrolyte (Fig. 2b), since low R_{ct} is beneficial for the kinetics of the battery reaction. As well known, the hydrated Zn^{2+} ($[Zn(H_2O)_6]^{2+}$) clusters are the general Zn-containing cations in dilute electrolyte

for aqueous Zn-metal batteries.[28-31] While, both the $[ZnCl(H_2O)_5]^+$ and $[Zn(H_2O)_6]^{2+}$ clusters are thermodynamically most stable in 1 M $ZnCl_2$ solutions.[32, 33] It has been reported that the dehydration process of $[ZnCl(H_2O)_5]^+$ clusters requires an lower energy than $[Zn(H_2O)_6]^{2+}$ clusters,[33] thus leading to a lower R_{ct} in the $ZnCl_2$ electrolyte than that in other three electrolytes. Hence, 1 M $ZnCl_2$ electrolyte among the investigated electrolytes is the most judicious choice for the Zn-S battery, and the following electrochemical measurements were based on 1 M $ZnCl_2$ aqueous solution as the electrolyte.

To discover the electrochemical behaviour of the sulfur cathode in the mildly acidic electrolyte (pH=4.08), the characterizations such as XRD, transmission electron microscopy (TEM), energy dispersive X-ray spectroscopy (EDX), and X-ray photoelectron spectroscopy (XPS) were conducted on the discharged cathode. The *ex*-situ XRD patterns revealed that the final discharge product harvested at the cut-off voltage of 0.1 V shows a ZnS phase, where the sulfur phase is completely consumed during the discharge process (Fig. 2c, S7). This is different from the reactions of the sulfur cathode that is coupled with the Zn or Al anode in alkaline electrolyte, in which the final sulfur-containing discharge product is H_2S.[34] The high revolution TEM (HR-TEM) image of the discharge product displayed the lattice spaces of 0.31 and 0.19 nm, which match with the (111) and (220) plane of ZnS (Fig. 2d). The elemental mapping for the discharged cathode demonstrated a uniform and overlapping distribution of both Zn and S elements (Fig. 2e). Meanwhile, the Zn/S molar ratio revealed by EDX is 1:0.9, which suggests the formation of ZnS as the final discharge product (Fig. S8). The *ex*-situ XPS measurement was further conducted for the S cathode at different states of charge (SOC) (Fig. 2f, S9 & S10). The S 2p spectrum of the pristine composite cathode shows the binding energies at 163 and 164 eV (Fig. 2f, S10), corresponding to the characteristic peaks of the elemental S in the cathode. After discharge, the sulfur peaks are replaced by a broad peak from 160 to 163.5 eV, which could be assigned to the sulfur in ZnS.[35] The characteristic peaks of Zn^{2+} were also observed in the Zn 2p spectrum, indicating the discharge-incorporated of Zn^{2+} in the composite cathode. It is worth noting that polysulfides were not detected by XPS in the discharged cathodes with different SOC, indicating the direct conversion reaction from sulfur to ZnS in the $ZnCl_2$ aqueous solution.[22] The lack of polysulfides is also supported by the characterization of the electrolyte by UV-Vis absorption, FT-IR, and Raman spectroscopic tools (Fig. S11).

A basic question is whether this Zn-S battery is rechargeable. We charged the battery to 1.5 V to evaluate the rechargeability of this Zn-S battery as shown in Fig. S12. Although the charge process achieves a reversible capacity of 1628 mAh g^{-1}, the full cycle suffers a large voltage hysteresis of 0.8 V between the charge and discharge curves, which results in an ultralow roundtrip efficiency of 30%. The discharge capacity rapidly decayed from 1668 mAh g^{-1} to 560 mAh g^{-1} after 4 cycles, this could be attributed to the irreversible formation of soluble $ZnSO_4$ from the oxidization of ZnS (Fig. S12a, 13), as reported in the previous work.[35] We previously reported a concentrated 30 m $ZnCl_2$ electrolyte featuring with high stability that may increase the stability of ZnS,[36] since the electrolyte also involves the oxidization process of ZnS to $ZnSO_4$.[37-39] Although the utilization of 30 m $ZnCl_2$ could increase the cycling

stability of S cathode, it also resulted in a low specific capacity and a large voltage hysteresis up to 0.95 V (Fig. S12c). Therefore, the rechargeability of Zn-S batteries using $ZnCl_2$ electrolyte should be further increased. The proposed electrochemical reactions in the aqueous Zn-S battery can be summarized as below:

Discharge process:

Cathode: $S + Zn^{2+} + 2e^- \rightarrow ZnS$

Anode: $Zn - 2e^- \rightarrow Zn^{2+}$

Charge process:

Cathode: $ZnS - 2e^- \rightarrow S + Zn^{2+}$

$2ZnS + 4H_2O - 10e^- \rightarrow 2Zn^{2+} + SO_4^{2-} + S + 8H^+$

Anode: $Zn^{2+} + 2e^- \rightarrow Zn$
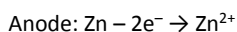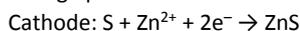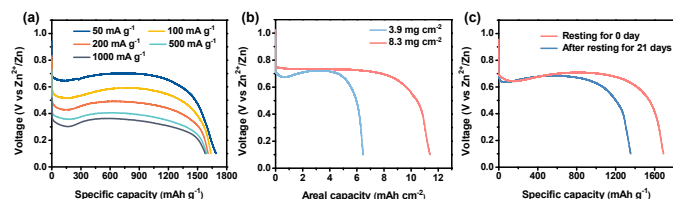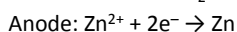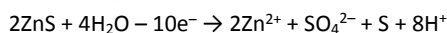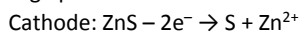
Fig. 3 (a) Rate capability of the Zn-S cells at different current rates. (b) Discharge profiles of the Zn-S cells with the sulfur mass loading of 3.9 and 8.3 mg cm^{-2}. (c) The self-discharge performance of Zn-S cell at a discharge current of 50 mA g^{-1}.

The rate performance for the Zn-S battery was evaluated at different current rates (Fig. 3a). The discharge voltage for the S cathode decreases from 0.68 V to 0.35 V with increasing the current rates from 50 to 1000 mA g^{-1}, which can be attributed to the increased polarization resulting from the strong interaction between S^{2-} and Zn^{2+}. This is very similar to that between S^{2-} and Al^{3+}.[40,41] The calculated diffusion coefficient for Zn^{2+} in the sulfur cathode is 1.22×10^{-13} cm^2 s^{-1} (Fig. S14).[42,43] Interestingly, the battery delivers the similar specific capacity at different currents.

For real-world applications, it is valuable that the electrode contains high mass loading of active materials. After increasing the mass loading of sulfur from 3.9 to 8.3 mg cm^{-2} in the cathode, a high specific capacity of 1375 mAh g^{-1} with an average voltage of 0.7 V still can be achieved, corresponding to a high areal capacity of 11.4 mAh cm^{-2} and an areal energy of 7.7 mWh cm^{-2}, both are rarely achieved by cathode materials in previously reported various primary batteries (Fig. 3b, S15, Tab. S1).

As for primary batteries, self-discharge behavior is also important to the practical application. This Zn-S primary battery exhibits a high capacity-retention of 80.1% after resting the battery for 21 days, revealing a moderate self-discharge rate (Fig. S16). The calendar life might be further increased by using solid or quasi-solid-state electrolytes that have been successfully applied in commercial alkaline Zn-MnO$_2$ batteries. The high energy density and low cost as well as excellent performance enable this Zn-S battery to offer a promising technique for high energy and cost-effective primary battery.

In summary, we report an aqueous primary battery by means of cost-effective sulfur cathode and Zn foil anode in different aqueous electrolytes. The comparative study revealed that the electrolyte shows a significant influence on both the discharge capacity and the plateau voltage. The 1 M $ZnCl_2$ electrolyte enables the S cathode to

deliver a high capacity of 1668 mAh g^{-1} with a high discharge plateau around 0.7 V. The *ex*-situ characterization on the discharge process demonstrated a direct conversion reaction from S to ZnS for the aqueous Zn-S chemistry. The sulfur cathode also can work at a high mass loading up to 8.3 mg with a specific capacity of 1375 mAh g^{-1}, corresponding to a high areal capacity of 11.4 mAh cm^{-2} and an areal energy of 7.7 mWh cm^{-2}. Benefiting from the natural abundance, low cost, and high energy density of sulfur cathode as well as the intrinsic safety of the aqueous electrolyte, the aqueous Zn-S chemistry offers a promising opportunity for cost-effective, high energy and environment-friendly primary battery.

Conflicts of interest

There are no conflicts to declare.

References

1. X. Ji, *Energy Environ. Sci*., 2019, 12, 3203-3224.

2. L. E. Blanc, D. Kundu and L. F. Nazar, *Joule*, 2020, 4, 771-799.

3. Y.-P. Deng, R. Liang, G. Jiang, Y. Jiang, A. Yu and Z. Chen, *ACS Energy Lett*., 2020, 5, 1665-1675.

4. D. Chao, W. Zhou, F. Xie, C. Ye, H. Li, M. Jaroniec and S.-Z. Qiao, *Sci. Adv*., 2020, 6, eaba4098.

5. L. Ma, S. Chen, N. Li, Z. Liu, Z. Tang, J. A. Zapien, S. Chen, J. Fan and C. Zhi, *Adv. Mater*., 2020, 32, 1908121.

6. W. Chen, X. Feng, J. Chen and L. Yan, *RSC Adv*., 2014, 4, 42418-42423.

7. A. P. Karpinski, B. Makovetski, S. J. Russell, J. R. Serenyi and D. C. Williams, *J. Power Sources*, 1999, 80, 53-60.

8. Y. Wei, Y. Shi, Y. Chen, C. Xiao and S. Ding, *J. Mater. Chem. A*, 2021, 9, 4415-4453.

9. F. Y. Cheng, J. Chen, X. L. Gou and P. W. Shen, *Adv. Mater*., 2005, 17, 2753-2756.

10. Y. Gao, H. Yang, Y. Bai and C. Wu, *J. Mater. Chem. A*, 2021, 9, 11472-11500.

11. W. Shi, W. S. V. Lee and J. Xue, *ChemSusChem*, 2021, 14, 1634-1658.

12. Sang H. Je, O. Buyukcakir, D. Kim and A. Coskun, *Chem*, 2016, 1, 482-493.

13. J.-G. Wagenfeld, K. Al-Ali, S. Almheiri, A. F. Slavens and N. Calvet, *Waste Manage*., 2019, 95, 78-89.

14. F. Jalilehvand, *Chem. Soc. Rev*., 2006, 35, 1256-1268.

15. X. Ji, K. T. Lee and L. F. Nazar, *Nat. Mater.*, 2009, 8, 500-506.

16. Y. Zhao, D. Wang, X. Li, Q. Yang, Y. Guo, F. Mo, Q. Li, C. Peng, H. Li and C. Zhi, *Adv. Mater.*, 2020, 32, 2003070.

17. P. Xiong, X. Han, X. Zhao, P. Bai, Y. Liu, J. Sun and Y. Xu, *ACS Nano*, 2019, 13, 2536-2543.

18. W. Ge, L. Wang, C. Li, C. Wang, D. Wang, Y. Qian and L. Xu, *J. Mater. Chem. A*, 2020, 8, 6276-6282.

19. R. Fang, J. Xu and D.-W. Wang, *Energy Environ. Sci.*, 2020, 13, 432-471.

20. Y. Yang, G. Zheng and Y. Cui, *Chem. Soc. Rev.*, 2013, 42, 3018-3032.

21. T. Liu, H. Hu, X. Ding, H. Yuan, C. Jin, J. Nai, Y. Liu, Y. Wang, Y. Wan and X. Tao, *Energy Stor. Mater.*, 2020, 30, 346-366.

22. X. Wu, A. Markir, Y. Xu, E. C. Hu, K. T. Dai, C. Zhang, W. Shin, D. P. Leonard, K.-i. Kim and X. Ji, *Adv. Energy Mater.*, 2019, 9, 1902422.

23. X. Yu and A. Manthiram, *Adv. Energy Mater.*, 2017, 7, 1700561.

24. H. Li, J. Lampkin and N. Garcia-Araez, *ChemSusChem*, 2021，DOI：10.1002/cssc.202100973

25. K. A. See, J. A. Gerbec, Y.-S. Jun, F. Wudl, G. D. Stucky and R. Seshadri, *Adv. Energy Mater.*, 2013, 3, 1056-1061.

26. X. Yu, M. J. Boyer, G. S. Hwang and A. Manthiram, *Adv. Energy Mater.*, 2019, 9, 1803794.

27. J. W. Gallaway, M. Menard, B. Hertzberg, Z. Zhong, M. Croft, L. A. Sviridov, D. E. Turney, S. Banerjee, D. A. Steingart and C. K. Erdonmez, *J. Electrochem. Soc.*, 2014, 162, A162-A168.

28. S. De, S. M. Ali, A. Ali and V. G. Gaikar, *Phys. Chem. Chem. Phys.*, 2009, 11, 8285-8294.

29. C. Nguyen-Trung, J. C. Bryan and D. A. Palmer, Struct. *Chem.*, 2004, 15, 89-94.

30. A. C. Hayes, P. Kruus and W. A. Adams, *J. Solution Chem.*, 1984, 13, 61-75.

31. C.-Y. Chen, K. Matsumoto, K. Kubota, R. Hagiwara and Q. Xu, *Adv Energy Mater.*, 2019, 9, 1900196.

32. D. J. Harris, J. P. Brodholt, J. H. Harding and D. M. Sherman, *Mol. Phys.*, 2001, 99, 825-833.

33. C. Wang, Z. Pei, Q. Meng, C. Zhang, X. Sui, Z. Yuan, S. Wang and Y. Chen, *Angew. Chem. Int. Ed.*, 2021, 60, 990-997.

34. D. Peramunage and S. Licht, *Science*, 1993, 261, 1029-1032.

35. W. Li, K. Wang and K. Jiang, *Adv. Sci.*, 2020, 7, 2000761.

36. C. Zhang, J. Holoubek, X. Wu, A. Daniyar, L. Zhu, C. Chen, D. P. Leonard, I. A. Rodríguez-Pérez, J.-X. Jiang, C. Fang and X. Ji, *Chem. Commun.*, 2018, 54, 14097-14099.

37. Q. Pang, D. Kundu, M. Cuisinier and L. F. Nazar, *Nat. Commun.*, 2014, 5, 4759.

38. G. Zhou, L.-C. Yin, D.-W. Wang, L. Li, S. Pei, I. R. Gentle, F. Li and H.-M. Cheng, *ACS Nano*, 2013, 7, 5367-5375.

39. L. Zhang, L. Ji, P.-A. Glans, Y. Zhang, J. Zhu and J. Guo, *Phys. Chem. Chem. Phys.*, 2012, 14, 13670-13675.

40. Y. Guo, H. Jin, Z. Qi, Z. Hu, H. Ji and L.-J. Wan, *Adv. Funct. Mater.*, 2019, 29, 1807676.

41. T. Gao, X. Li, X. Wang, J. Hu, F. Han, X. Fan, L. Suo, A. J. Pearse, S. B. Lee, G. W. Rubloff, K. J. Gaskell, M. Noked and C. Wang, *Angew. Chem. Int. Ed.*, 2016, 55, 9898-9901.

42. C. Ho, I. D. Raistrick and R. A. Huggins, *J. Electrochem. Soc.*, 1980, 127, 343-350.

43. Y. Cui, X. Zhao and R. Guo, *Electrochim. Acta*, 2010, 55, 922-926.